2013 IEEE 10th International Symposium on Biomedical Imaging:
From Nano to Macro
San Francisco, CA, USA, April 7-11, 2013

TUMOR GROWTH MODELING BASED ON DUAL PHASE CT AND FDG-PET

Yixun Liu[1], Samira M. Sadowski[2], Allison B. Weisbrod[2], Electron Kebebew[2], Ronald M. Summers[1] and Jianhua Yao[1]

[1]Clinical Image Processing Service, Radiology and Imaging Sciences, NIH
[2]Endocrine Oncology Branch, National Cancer Institute, NIH

ABSTRACT

In this paper, we presented a method to deal with tumor growth prediction using multimodality non-invasive clinical imaging data. We developed a reaction-diffusion tumor growth model that (1) relates cell metabolic rate and tumor growth, and (2) is driven by clinical imaging data. The metabolic rate was incorporated into the model through cell proliferation rate of the model via energy conservation law. FDG-PET scan was employed to provide non-invasive measurement of the metabolic rate. To bridge the gap between the model prediction and the clinical observation, we introduced intracellular volume fraction (ICVF) using dual phase CT scans to link them. The patient specific model parameters were estimated by minimizing the deviation between the predicted ICVF and the measured ICVF with deformation corrected.

The experiment was conducted on two pancreatic neuroendocrine tumors. The average surface distance between the predicted tumor and the reference tumor was 2.1 mm and 2.7 mm, respectively, and the mean square difference of the ICVF map was 5.4% and 3.8%, respectively.

Index Terms—Tumor growth, image driven, reaction-diffusion model, metabolic rate, intracellular volume fraction

1. INTRODUCTION

Reaction-diffusion systems, originally introduced by Turing over 50 years ago [1], play a fundamental role in modeling spatial-temporal dynamics in system biology. The reaction-diffusion model describes the change of the cell population using a partial differential equation (PDE). Recently, this model has been adopted to study tumor growth [2] [3] [4]. Swanson et al. assumed an infiltrative growth of the tumor cells, while considering differences in cell diffusion in white and gray matter [4]. Clatz et al. modeled locally anisotropic migration patterns by integrating information from diffusion tensor images (DTI) [3]. Davatzikos et al. [2] and Clatz et al. [3] included the mechanical properties of the lesion on surrounding structures to model mass effect. Ontogenetic development is fuelled by metabolism and occurs primarily by cell division. West et al. [5] presented a general model for ontogenetic growth based on the allometric law and energy conservation law. The incoming metabolic energy is allocated to two parts: one part for the maintenance of the existing cells and the other part for the creation of new cells. This work was further extended by Alexander et al. to study the relationship between tumor vascularization and growth to metabolic rate [6]. In this paper, we derive a quantitative relation between the metabolic rate and cell proliferation rate of the reaction-diffusion model via the energy conservation law, yielding a model relating tumor growth and cell metabolic rate and cell infiltration.

To measure the metabolic rate, we used FDG-PET (2-[18F] Fluoro-2-deoxyglucose positron emission tomography) due to its wide availability in oncology to find regions in the body which are more active and need more energy. The energy for organism growth is supplied by different metabolic pathways. The metabolic energy of the tumor can be approximated by that supplied by glycolytic pathway due to the established model of the Warburg effect: cancer cells use glycolysis for energy production regardless of the availability of oxygen because glycolysis produces energy much faster than oxidative phosphorylation despite the loss in efficiency [7]. Tracer kinetic modeling is a formal way to calculate glucose metabolic rate [8]; however, this modeling approach usually requires taking series of blood samples from the studied subject to give the time course of the tracer delivery, and requires measuring the dynamics of the radiolabel in local tissues. Standardized Uptake Value (SUV) is a semi-quantitative measurement of the metabolic rate and does not need dynamic blood sampling and PET scanning, therefore is extremely suitable for routine clinical use. In this paper, we present the relation between both glucose metabolic rate and SUV, and the proliferation rate.

The reaction-diffusion model describes the change of the cell population, which is not directly measurable by the non-invasive imaging data. To bridge the gap between the model and the clinical images, we introduced intracellular volume fraction. On the image side, we used dual phase CT images to measure the ICVF, and on the model side, we adapted the model to predict the ICVF rather than the cell population.

The patient specific model parameters were estimated by minimizing the deviation between the predicted ICVF and the measured ICVF. To deal with the deformation between two successive longitudinal ICVFs, an additional transformation variable was introduced into the parameter estimation framework to allow a simultaneous estimation of the transformation and the model parameter using an alternating optimizer [9].

2. METHOD

In this section, we first derive a reaction-diffusion model with cell metabolic rate incorporated via cell metabolic rate conservation law; and then describe how to use FDG-PET to measure the metabolic rate and SUV, and how to use dual phase CT to measure ICVF; finally, we present an energy function to simultaneously estimate unknown model parameters and potential deformation.

2.1 Model derivation

According to the tumor logistical growth law presented in [10], the number of the newly created cells can be described by,

$$\frac{dN}{dt} = \rho N(1 - \frac{N}{K}) \tag{1}$$

where N is the number of cells, a function of time t. ρ is spatial-temporal invariant proliferation rate. This law describes that the tumor grows exponentially at the beginning and then gradually slows down as approaching the carrying capacity K.

As a tumor progresses, the parts with sufficient nutrient grow faster, and the parts suffering vascular inefficiencies will develop into necrosis [11], suggesting a heterogeneous spatial-temporal proliferation function $\rho(\boldsymbol{x}, t)$. The metabolic energy conservation law presented by West et al. [5] quantitatively describes the relationship between the metabolic energy and the tumor growth, providing the theoretical foundation to explore the heterogeneity of the proliferation rate. The energy conservation law states that the incoming energy $B(t)$ required for tumor growth is allocated to two parts,

$$B = NB_m + E_c \frac{dN}{dt} \tag{2}$$

where the first term represents the energy to maintain the existing cells and the second term represents the energy to create new cells. B_m is the energy each cell required for maintenance, and E_c is the energy required to create a cell. Both B_m and E_c are constant during tumor growth. Replace $\frac{dN}{dt}$ in equation (2) with $\rho N(1 - \frac{N}{K})$,

$$\begin{aligned} B &= NB_m + E_c \rho N(1 - \frac{N}{K}) \\ \rightarrow \rho &= \frac{KB - KB_m N}{E_c N(K - N)} \end{aligned} \tag{3}$$

The proliferation rate ρ in equation (3) is a function of time t. However, in clinical practice, ρ is only available at specific time points, when B and N are measurable. Thus, we approximate ρ at time t between 0 and T with a linear interpolation,

$$\rho(t) = \rho(0) + \frac{t}{T}\big(\rho(T) - \rho(0)\big) = \frac{KB(0) - KB_m N(0)}{E_c N(0)(K - N(0))} + \frac{t}{T}\left(\frac{KB(T) - KB_m N(T)}{E_c N(T)(K - N(T))} - \frac{KB(0) - KB_m N(0)}{E_c N(0)(K - N(0))}\right) \tag{4}$$

Apply model (1) to each voxel (millions of cells within $1mm^3$) with position $\boldsymbol{x}$, and add a diffusion term as that in the reaction-diffusion model [1] to account for cancerous cell infiltration into surrounding tissues, leading to a reaction-diffusion model,

$$\frac{\partial N}{\partial t} = D\nabla^2 N + \rho N(1 - \frac{N}{K}) \tag{5}$$

where the first term is the diffusion term, and the second term is the reaction (proliferation) term. D is the diffusivity or infiltration rate. Equation (5) describes that the rate of cell number change equals the sum of the net dispersal of cancer cells and the net proliferation of cancerous cells. Note that both $N$and ρ are a function of position $\boldsymbol{x}$ and time t. $\rho(\boldsymbol{x}, t)$ depends on metabolic rate maps and ICVF maps at time 0 and T, which can be measured by FDG-PET and dual phase CT, respectively.

Because the cell number N is difficult to be directly measured by imaging data, we adapt equation (5) by letting $N(x, t) = Ku(x, t)$, where u is the intracellular volume fraction within a voxel, which is observable by dual phase CT images to be explained in Section 2.3,

$$\frac{\partial u}{\partial t} = D\nabla^2 u + \rho u(1 - u) \tag{6}$$

where (replace N in (4) with Ku)

$$\rho(\boldsymbol{x}, t) = \frac{B(0) - au(0)}{bu(0) - bu^2(0)} + \frac{t}{T}\left(\frac{B(T) - au(T)}{bu(T) - bu^2(T)} - \frac{B(0) - au(0)}{bu(0) - bu^2(0)}\right) \tag{7}$$

where $a = KB_m$ and $b = KE_c$. Position $\boldsymbol{x}$ is omitted in the left side. Both parameters a and b have specific biological meanings, representing the energy to maintain K cells and create K cells, respectively. The proposed model (6) has similar format with the reaction-diffusion model used in [2] [3] [4], but it differs from them in relating metabolic rate to tumor growth and being driven by clinical imaging data.

To estimate unknown parameters a, b and D, we need to measure metabolic rate B and intracellular volume fraction u.

2.2 Measure B using FDG-PET

The formal way to calculate glucose metabolic rate, an approximation of metabolic rate B, was originally presented in [8], in which the glucose metabolic rate MR_{glc} can be precisely calculated by,

$$MR_{glc} = B = \frac{1.0}{LC}\frac{K_1 K_3}{K_2 + K_3} Glc \tag{8}$$

where LC is a lumped constant that accounts for the transport and phosphorylation difference between FDG and glucose, and Glc is the glucose concentration in arterial plasma. $[K_1 K_3/(K_2 + K_3)]$ (commonly called the uptake constant) can be estimated given dynamic FDG-PET scans and blood samples, usually not available in routine clinical practice. Normally, when the scanning time is longer than 45 min post-injection, the uptake constant can be approximated by [12],

$$\frac{K_1 K_3}{K_2 + K_3} = \frac{PET(t)}{k \cdot (dose)/(body\ weight)} \tag{9}$$

where $PET(t)$ denotes the radioactive tracer FDG^{18} concentration in tissue at time t that is measurable with PET. k (b in [12]) is a constant that is not dependent on the particular subject being studied. Replace the uptake constant in (8) with (9),

$$MR_{glc} = \frac{\frac{Glc}{100.0} \cdot PET(t)/(\frac{dose}{body\ weight})}{LC \cdot k/100.0} \rightarrow MR_{glc} = B = c \times SUV(t) \quad (10)$$

where $c = \frac{1.0}{LC \cdot k/100.0}$, a lumped unknown parameter. Note that the numerator in (10) is widely used as SUV, which is proportional to MR_{glc} since both *k* and *LC* are constants [12].

2.3 Measure *u* using pre- and post-contrast CT images

A tissue within a voxel is considered to be made of three well-defined regions: (1) a vascular space through which the blood flows; (2) an extravascular extracellular space (EES) which provides the supporting structure of the tissue; and (3) the cellular space. Because iodinated contrast medium is constrained in the extracellular volume (ECV, vascular space plus EES), and the amount of the contrast within a voxel is proportional to the CT enhancement [13], we can calculate the extracellular volume fraction (ECVF, the complement of ICVF) of the studied voxel by normalizing its enhancement with the enhancement of a reference voxel, which only has contrast and the concentration is the same as that in the ECV of the studied voxel, as shown in equation (11),

$$ECVF(t) = \frac{CT_{post}(t) - CT_{pre}(t)}{(HU_{post\_ploodpool} - HU_{pre\_ploodpool})/(1.0 - Hct_{blood})} \quad (11)$$

where the numerator is the enhancement brought by the contrast distributed in the ECV of the studied voxel, and the denominator is the enhancement brought by the contrast distributed in the whole voxel of the reference voxel. When reaching equilibrium, both the numerator and the denominator are proportional to the volume of the space. In fact, there is no such kind of voxels with only contrast, but we can use the voxel in the blood pool of the heart as the reference voxel as [14] since we know the percentages of the plasma and the red blood cells in the voxel. $\Delta HU = HU_{post\_bloodpool} - HU_{pre\_bloodpool}$ is the enhancement brought by the plasma, which accounts for $1.0 - Hct_{blood}$ percentage of the voxel. The hematocrit Hct_{blood} is the volume percentage (%) of red blood cells in blood, which can be measured by the blood sample. ECVF's complement ICVF can be calculated by,

$$u(t) = 1.0 - ECVF(t) \quad (12)$$

Replacing *B* in equation (7) with $c \times SUV(t)$, and measuring u using equation (12) at time 0 and *T*, equation (7) changes to,

$$\rho(\boldsymbol{x}, t) = \frac{\alpha SUV(0) - \beta u(0)}{u(0) - u^2(0)} + \frac{t}{T}\left(\frac{\alpha SUV(T) - \beta u(T)}{u(T) - u^2(T)} - \frac{\alpha SUV(0) - \beta u(0)}{u(0) - u^2(0)}\right) \quad (13)$$

where $\alpha = c/b, \beta = a/b$. Equation (7) is suitable for the dynamic FDG-PET scans with *B* measured by a tracer kinetic model, and equation (13) is suitable for static FDG-PET scan with SUV as a semi-quantitative measurement of *B*. $\rho(\boldsymbol{x}, t)$ is the generalization of spatial-temporal invariant ρ in equation (1), leading to a heterogeneous growth model (6). In equation (13), when $\frac{SUV(T)-u(T)}{u(T)-u^2(T)} = \frac{SUV(0)-u(0)}{u(0)-u^2(0)} = constant$ for all position $\boldsymbol{x}$ and $\alpha = \beta$, $\rho(\boldsymbol{x}, t)$ is reduced to $\frac{\alpha(SUV(0)-u(0))}{u(0)-u^2(0)}$ (equivalent to constant ρ), leading to the homogeneous model (1). The benefit using energy conservation law (2) to explore the heterogeneity of the proliferation rate lies in the removal of the influence of the cell number. For instance, a higher FDG-PET value heuristically denotes a more aggressive growth. But, this aggressiveness can be caused by more less-aggressive cells or less more-aggressive cells. Thus, simply weighting the proliferation rate with the PET value cannot truly reflect the aggressiveness of the growth.

2.4 Parameter estimation

Problem definition: Given measured SUV: $SUV(0), SUV(T)$, *and measured ICVF:* $u(0), u(T)$ *at time 0 and T, simultaneously estimate transform U and model parameters:* α, β *and* D.

We introduce transform $U(\boldsymbol{x})$ in order to track the movement of each voxel from time 0 to time *T*. The unknown parameters are estimated by minimizing the mean of the sum of the square of the deviation between the measured ICVF $u(\boldsymbol{x_i}, T)$ and the predicted and deformed ICVF $u'(U(\boldsymbol{x_i}), T)$,

$$\frac{1}{M}\sum_i \|u'(U(\boldsymbol{x_i}), T) - u(\boldsymbol{x_i}, T)\|^2 \quad (14)$$

where *i* is the index of the voxel, and $\boldsymbol{x_i}$ is the position of the *i*-th voxel. *M* is the number of voxels. The predicted $u'(\boldsymbol{x_i}, T)$ is the solution of the proposed PDE model (6) with proliferation rate (13) and the initial condition: $u_0 = u(0)$, actually leading energy function (14) to a PDE-constrained optimization problem. We use backward Euler finite difference method (FDM) to get the numerical solution u', and use free-form deformation (FFD) to simulate transform U. The two physically different parameters $< \alpha, \beta, D >$ and U are estimated by an alternating optimizer [9].

3. RESULTS

Two patients both with pathologically confirmed pancreatic neuroendocrine tumors were enrolled in our experiment with their written consent. Patient information is listed in Table 1. Fig.1 shows the tumor in the longitudinal post-contrast CT and the corresponding ICVF. The parameters for ICVF calculation and the range of ICVF are listed in Table 2.

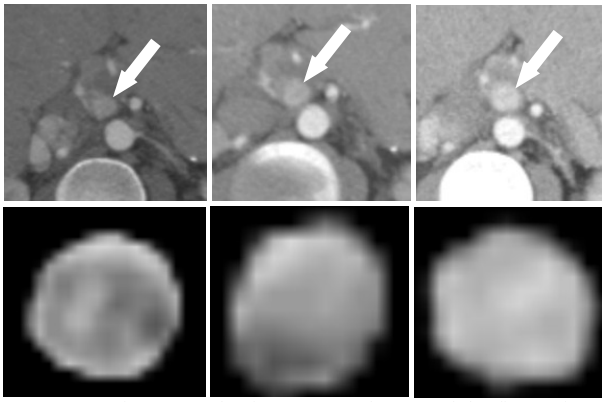

Figure 1. Pancreatic neuroendocrine tumor and ICVF of the first patient. The first row shows tumors at baseline (*T=0* day), 1st follow-up (*T=248* days), and 2nd follow-up (*T=606* days) in the post-contrast CT. The second row shows corresponding ICVF.

The left part of Fig. 2 shows fused FDG-PET and CT, and the measured SUV maps at baseline and the 1st follow-up. Corresponding parameters and SUV range are listed in Table 2. The ICVF and SUV maps at baseline and the 1st follow-up are used to estimate the model parameters, and the ICVF at the 2nd follow-up is used to compare with the predicted ICVF. The right part of Fig.2 shows the comparison between the ICVF at the 2nd follow-up and the predicted ICVF.

Table 1. Patient information. The scanning time is relative to the baseline ($T=0$) with unit days.

Id	*Age*	*Gender*	*Location*	*Grade*	*#Tumor*	*Base*	*1st*	*2nd*
1	36	female	head	3	1	0	248	606
2	35	male	head/uncinate	3	2	0	365	729

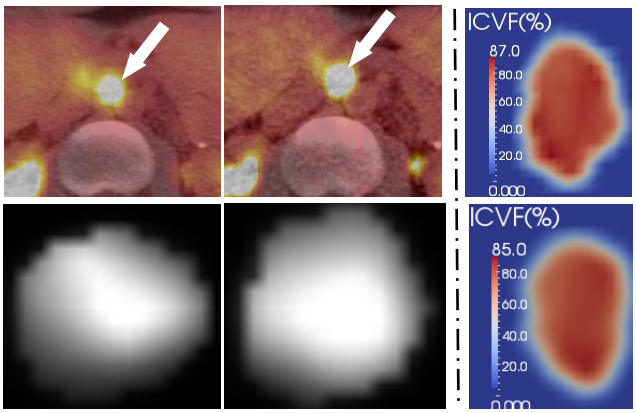

Figure 2. Left: FDG-PET and measured SUV maps of the first patient. The first row shows the fused FDG-PET at baseline and the 1st follow-up, and the second row shows corresponding measured SUV maps of the segmented tumor. Right: the ICVF at the 2nd follow-up (top) and the predicted ICVF (bottom).

Fig.3 shows the predicted tumor, which was produced by growing the tumor from the 1st follow-up for 358 days with the estimated parameters listed in Table 1. When we performed prediction, we did not use the FDG-PET at the 2nd follow-up and assumed the estimated proliferation rate map to be fixed from the 1st follow-up to the 2nd follow-up.

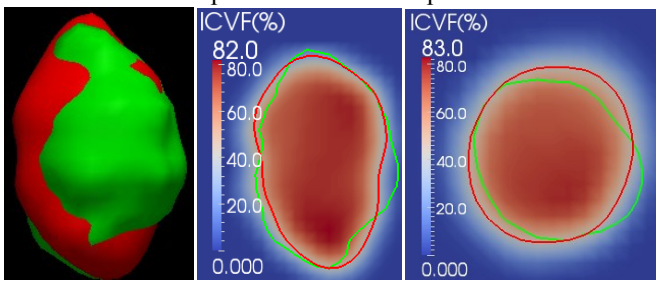

Figure 3. Prediction results of the first patient. Left: the predicted tumor (red) and the reference tumor (green, 2nd follow-up). The predicted tumor is the isosurface of ICVF 41.5%, which is the average ICVF of the surface of the reference tumor. The middle figure shows the isocontour (red) of the predicted tumor and the boundary (green) of the reference tumor from the coronal view. The right figure is the transversal view. The background images in the middle and the right figures are the predicted ICVF cross-sections.

Table 2. Measured ICVF, SUV and prediction evaluation. ICVF: Hct comes from blood samples, ΔHU is the average enhancement of the voxels located in the blood pool. SUV: Glc is not included in the SUV calculation. Prediction: ASD: average surface distance, MSD: mean square difference. Unit: ICVF(%), Dose(MBq), Weight(Kg), SUV(g/ml), D(mm^2/day), ASD(mm), MSD(%). Different colors denote different patients.

ICVF				SUV			Prediction	
	base	1st	2nd		base	1st		
Hct	0.42	0.41	0.42	Dose	397.38	397.38	$\alpha(10^{-6})$	6.3
							$\beta(10^{-6})$	57.2
ΔHU	279	230	252	Weight	73.0	72.0	D	.002
							ASD	2.1
ICVF	[0,81]	[0,86]	[0,87]	SUV	[0,14.5]	[0,18.4]	MSD	5.4
Hct	0.43	0.43	0.45	Dose	356.31	360.38	$\alpha(10^{-6})$	3.5
							$\beta(10^{-6})$	43.6
ΔHU	356	122	268	Weight	74.0	76.8	D	.002
							ASD	2.7
ICVF	[0,58]	[0,61]	[0,70]	SUV	[0,6.0]	[0,7.8]	MSD	3.8

4. CONCLUSIONS

In this paper, we presented a method to deal with tumor growth prediction using multimodality images. On the model side, we derived a reaction-diffusion model to incorporate information from different aspects such as cell volume fraction and metabolic rate. On the image side, we used different modality images to measure what the model requires and predicts such as using FDG-PET to measure metabolic rate/SUV and using dual phase CT to measure ICVF. The preliminary experiment on pancreatic neuroendocrine tumors demonstrated the promise of the method.

REFERENCES

[1] A.M. Turing, "The chemical basis of morphogenesis," *Philosophical Transactions of the Royal Society of London*, vol. 237, no. 641, pp. 37-72, 1952.

[2] C. Hogea, C. Davatzikos, and G. Biros, "An image-driven parameter estimation problem for a reaction-diffusion glioma growth model with mass effects," *J Math Biol*, vol. 56, pp. 793-825, 2008.

[3] O. Clatz et al., "Realistic simulation of the 3-D growth of brain tumors in MR images coupling diffusion with biomechanical deformation," *IEEE Transactions on Medical Imaging*, vol. 24, pp. 1334-1346, 2005.

[4] K.R. Swanson, E.C. Alvord, and J.D. Murray, "A quantitative model for differential motility of gliomas in grey and white matter," *Cell Prolif*, vol. 33, pp. 317-329, 2000.

[5] Geoffrey B. West, James H. Brown, and Brian J. Enquist, "A general model for ontogenetic growth," *Nature*, vol. 413, pp. 628-631, October 2001.

[6] Alexander B. Herman, Van M. Savage, and Geoffrey B. West, "A Quantitative Theory of Solid Tumor Growth, Metabolic Rate and Vascularization," *PLoS ONE*, vol. 6, no. 9, pp. 1-9, September 2011.

[7] Warburg O, "On the origin of cancer cells," *Science* , vol. 123, no. 3191, pp. 309–314, 1956.

[8] S. C. Huang et al., "Noninvasive determination of local cerebral metabolic rate of glucose in man," *Am J Physiol Endocrinol Metab*, vol. 238, pp. E69-E82, 1980.

[9] Attouch H, Bolte J, Redont P, and Soubeyran A, "Proximal alternating minimization and projection methods for nonconvex problems," *Mathematics of Operations*, vol. 35, no. 2, pp. 438-457, 2010.

[10] Michael Olinick, *An Introduction to Mathematical Models in the Social and Life Sciences*.: Addison-Wesley, 1978.

[11] Holland-Frei, *Cancer Medicine*, 6th ed.: Hamilton , 2003.

[12] (Henry) Sung-Cheng Huang, "Anatomy of SUV," *Nuclear Medicine & Biology*, vol. 27, pp. 643–646, 2000.

[13] Kyongtae T. Bae, "Intravenous Contrast Medium Administration and Scan Timing at CT: Considerations and Approaches," *Radiology*, vol. 256, pp. 32-61, 2010.

[14] Nacif MS et al., "Interstitial myocardial fibrosis assessed as extracellular volume fraction by low radiation dose cardiac ct," *Radiology*, vol. 264, no. 3, pp. 876-83, Sep. 2012, in press.